Earth and Planetary Science Letters 317-318 (2012) 436–445

Contents lists available at SciVerse ScienceDirect

Earth and Planetary Science Letters

journal homepage: www.elsevier.com/locate/epsl

Epeirogeny or eustasy? Paleozoic–Mesozoic vertical motion of the North American continental interior from thermochronometry and implications for mantle dynamics

Rebecca M. Flowers [a,*], Alexis K. Ault [a], Shari A. Kelley [b], Nan Zhang [c], Shijie Zhong [c]

[a] Department of Geological Sciences, University of Colorado, Boulder, CO, USA
[b] Earth and Environmental Sciences Department, New Mexico Institute of Mining and Technology, Socorro, NM, USA
[c] Department of Physics, University of Colorado, Boulder, CO, USA

ARTICLE INFO

Article history:
Received 19 August 2011
Received in revised form 16 November 2011
Accepted 18 November 2011
Available online 24 December 2011

Editor: R.W. Carlson

Keywords:
thermochronology
thermochronometry
Craton
dynamic topography
geodynamic modeling
(U–Th)/He

ABSTRACT

Geodynamic models predict that deep mantle buoyancy forces exert important control on the vertical motion history of continents, but it is difficult to isolate the effects of dynamic topography in the geologic record. Here we apply low temperature thermochronometry to exposed Precambrian basement samples across an ~1300 km long tract of the western Canadian shield to resolve the thermal imprint, thickness, spatial extent, and evolution of missing portions of the Phanerozoic sedimentary record. New and published apatite (U–Th)/He and fission-track data from three study areas indicate a pronounced heating and cooling event in Paleozoic–early Mesozoic time. This pattern, coupled with geologic observations, indicates that an extensive region of the continent was inundated and buried by sedimentary rocks in Paleozoic time, followed by significant Paleozoic–early Mesozoic unroofing that removed these strata from the rock record. This burial and unroofing history is opposite that expected from eustatic sea level chronologies. A process that can induce long-wavelength (>1000 km) elevation change in a continental interior region without significant crustal deformation therefore appears required to explain our results. These characteristics of the vertical motions largely eliminate plate margin tectonism as a probable mechanism, and point toward dynamic topography as a likely cause.

To evaluate the hypothesis of a dynamic control on the rise and fall of this cratonic region, we compare the 400 to 150 Ma burial and unroofing histories with the evolution of dynamic topography in the western Canadian shield predicted by a three-dimensional model of thermochemical convection. The histories of burial and unroofing mimic the predicted history of elevation change to first order, indicating that dynamic topography is a viable cause for the vertical motions. A phase of significant burial before ~350 Ma may be due to cold mantle downwellings that produced subsidence during Pangea assembly, followed by unroofing between ~350 Ma and 250 Ma induced by development of warm mantle upwellings after Pangea amalgamation. While a fuller range of mantle dynamic models must be explored to more completely understand the causes of cryptic elevation change in the North American continental interior, our study highlights the utility of cratonic thermochronometry data for testing and calibrating dynamic models, and for evaluating mantle and surface process interactions deep in Earth history.

1. Introduction

The idea that changing patterns of mantle flow influence the elevation history of continents has emerged as one of the significant geodynamic hypotheses of the last two decades (e.g., Gurnis, 1993; Hager and Richards, 1989; Lithgow-Bertelloni and Gurnis, 1997; Liu et al., 2008; Mitrovica et al., 1989; Moucha et al., 2008; Ricard et al., 1984; Ricard et al., 1993). Models predict that dynamic topography is transient with slow rates of change, and characterized by maximum vertical displacements of ~1000 m distributed over hundreds to thousands of kilometers (Braun, 2010). However, such models are difficult to test because of the challenge of unambiguously isolating modern and past topographic anomalies supported by mantle buoyancy forces from those due to tectonically induced differences in crustal and lithospheric thickness.

Teasing out the effects of dynamic topography in the geologic record is arguably best accomplished within continental interior settings where cryptic "epeirogenic" vertical displacements are not easily explained by plate margin tectonism. An example is the broad low degree tilt of thick Late Cretaceous sequences within the North American interior that can be accounted for by models in which subduction-induced changes in mantle flow patterns caused long wavelength subsidence followed by uplift of the continent (Liu et al., 2008; Mitrovica et al., 1989; Spasojevic et al., 2009). These Cretaceous strata are part of a thicker package of Phanerozoic sedimentary rocks that overlie much of the North American cratonic interior

* Corresponding author.
E-mail address: rebecca.flowers@colorado.edu (R.M. Flowers).

0012-821X/$ – see front matter © 2011 Elsevier B.V. All rights reserved.
doi:10.1016/j.epsl.2011.11.015

(Sloss, 1963). A longstanding debate exists over whether vertical cratonic motions (Algeo and Seslavinsky, 1995; Bond and Kominz, 1991) attributable to dynamic topography must also be invoked to explain the distribution of the Paleozoic cratonic sequences (Burgess and Gurnis, 1995; Pysklywec and Mitrovica, 2000), or if eustatic sea level change alone can account for their deposition (Sleep, 1976).

Here we address this problem by applying low temperature thermochronometry to exposed Proterozoic and Archean basement samples from an ~1300 km long swath of the western Canadian shield (Fig. 1). New and published apatite (U–Th)/He (AHe) and apatite fission-track (AFT) data better resolve the evolution of missing portions of the stratigraphic record across this cratonic interior region. Although mantle dynamic studies use the preserved sedimentary record to constrain continental uplift and subsidence episodes with which to calibrate dynamic models (Gurnis, 1993; Pysklywec and Mitrovica, 2000), an intrinsic limitation of this approach is that strata deposited during an ephemeral phase of dynamic subsidence are likely to be eroded during subsequent surface uplift, thus removing critical information about the burial and unroofing history from the rock record (Burgess and Gurnis, 1995). Our study addresses this shortcoming because the sensitivity of the AHe and AFT methods to 120–30 °C temperatures enables resolution of shallow (1–6 km) depositional and erosional episodes, even if the rocks associated with those events are no longer preserved. We then evaluate the processes responsible for the burial and unroofing histories inferred from the thermochronometry data by considering Paleozoic sea level curve reconstructions and the vertical motion history predicted for this region by a global mantle dynamic model. Our approach differs from past work in comparing directly the thermochronologically-constrained burial and unroofing histories over time with the evolution of predicted dynamic topography, rather than evaluating the consistency of model predictions with thermochronometry constraints at particular points in time (e.g., Spasojevic et al., 2009). In this manuscript we refer to “subsidence” and “uplift” or “surface uplift” as the decrease or increase in elevation of the Earth's surface, respectively. We refer to “burial” and “unroofing” as the addition or

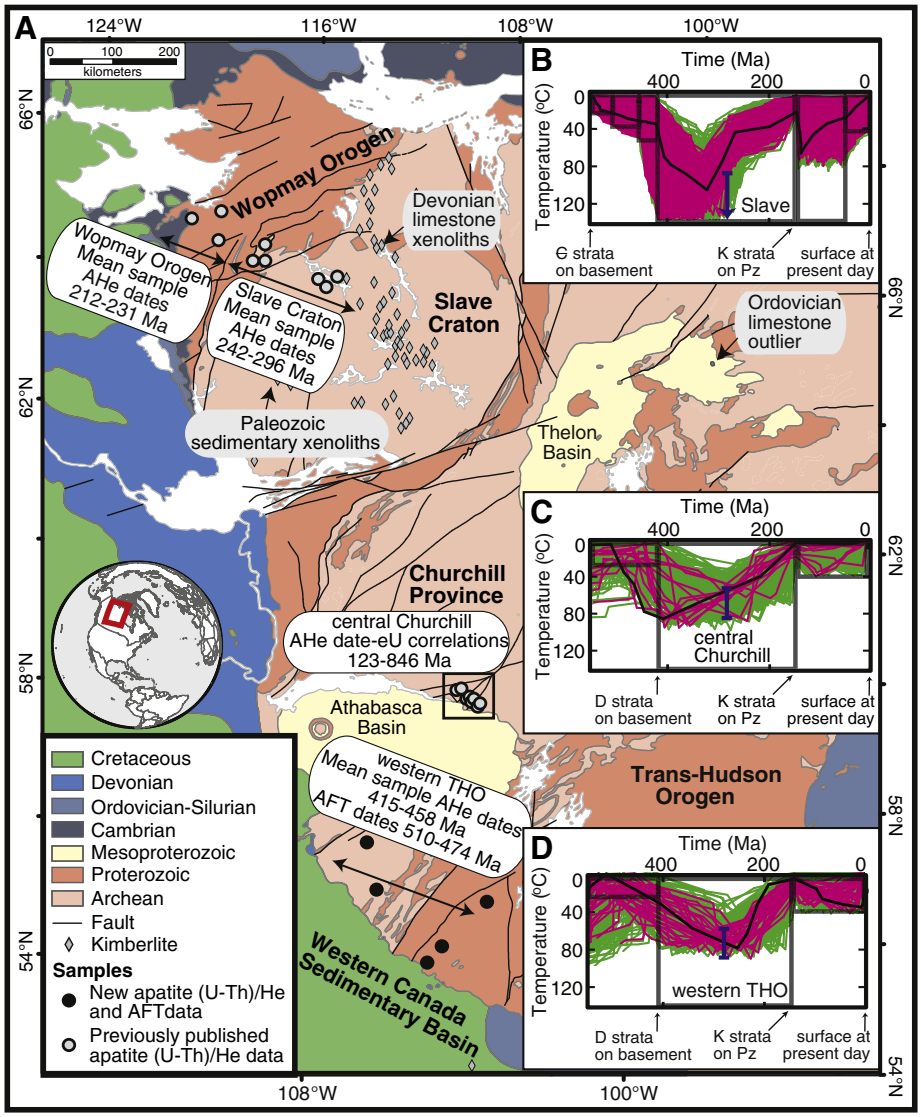

Fig. 1. (A) Simplified geologic map with thermochronometry results. Locations of Paleozoic sedimentary xenoliths entrained in kimberlite pipes and Ordovician limestone outlier are marked. Post-540 Ma inverse modeling simulation results are depicted as individual time-temperature paths for (B) Slave craton, (C) central Churchill Province, and (D) western THO. Gray rectangles are constraints imposed on thermal histories. Pink and green lines are good and acceptable fits. Black line is best-fit history. Blue brackets represent peak Paleozoic temperature range from the good fit histories.

removal of rocks or sediments at the Earth's surface, in this setting due to deposition or erosion, respectively.

2. Geologic setting

The western Canadian shield is a collage of Archean cratons that was assembled in the Proterozoic (Fig. 1). The region is underlain by a thick lithospheric mantle root and has remained structurally coherent and "cratonic" since Laurentian supercontinent development at ca. 1.7 Ga (Godey et al., 2004; Hoffman, 1989). The Slave craton in the northwestern Canadian shield consists of Archean and Proterozoic rocks as old as 4.0 Ga, is bounded by Proterozoic orogenic belts, and was pierced episodically by kimberlites during its history. The Wopmay orogen is a north-trending Paleoproterozoic orogenic belt that bounds the Slave craton to the west. The central Churchill Province contains Archean and Proterozoic rocks located to the southeast of the Slave craton. The Trans-Hudson Orogen (THO) is a Proterozoic orogenic belt that sutured the Churchill Province and Superior craton. The Proterozoic orogenic belts were active during Canadian shield amalgamation and ultimately became part of the larger cratonic region that now forms the Canadian shield.

Extensive regions of the western Canadian shield are currently devoid of Phanerozoic cover. However, Phanerozoic strata of the well-studied Western Canada Sedimentary Basin unconformably overlie the shield to the west (Fig. 1). This basin is a northeastward tapering wedge of sedimentary rocks that thickens westward to ~5 km at the eastern edge of the Cordillera (Wright et al., 1994). Clasts of Phanerozoic sedimentary xenoliths are entrained in kimberlite pipes of varying age in the Slave craton, indicating that Paleozoic and Mesozoic strata once buried the region (Cookenboo et al., 1998; Pell, 1996). In addition, an outlier of Ordovician marine limestone crops out east of the Slave craton >700 km from similar exposures in the Western Canada Sedimentary Basin, suggesting that these units were formerly much more extensive than at present (Wheeler et al., 1996; Wright, 1955).

3. AHe and AFT thermochronometry datasets

In this study we consider both previously published thermochronometry data from the northwestern Canadian shield and central Churchill Province, and new data from the THO, that together allow us to evaluate burial and unroofing patterns across an ~1300 km long corridor of the western Canadian shield (Fig. 1). Nine samples from a >250 km long transect across the Slave craton and Wopmay orogen yielded Permo-Triassic AHe results (Ault et al., 2009). Eight samples from the East Lake Athabasca region of the central Churchill Province yielded AHe date-eU correlations with individual dates ranging from Mesozoic to Precambrian (Flowers, 2009). We acquired new thermochronometry data for five Proterozoic basement samples collected within an ~265 km long region across the western THO (Tables 1 and 2). AHe and AFT data were acquired at Caltech and New Mexico Tech, respectively, following methods described in Flowers (2009) and Kelley et al. (1992). Sample lithologies consisted of gneiss, tonalite, granite, amphibolite, and meta-arkose. Mean sample AHe dates ranged from 458 ± 65 Ma to 399 ± 47 Ma, reported as the sample mean and 1-sigma sample standard deviation. The dated apatites are characterized by a restricted span (5–24 ppm) of effective uranium concentration (eU, weights U and Th for their alpha productivity, computed as [U] + 0.235[Th]) and do not display a strong correlation between AHe date and eU. AFT dates for four of these samples range from 474 ± 23 Ma to 510 ± 25 Ma, with uncertainties reported as the 1-sigma standard error of the pooled fission-track dates. The samples are characterized by slightly broad unimodal track length distributions with mean track lengths from 10.7 to 13.2 um (Fig. S1). The fifth sample yielded a mean date of 353 ± 20 Ma, distinctly younger than

Table 1
Apatite (U–Th)/He data from the western Trans-Hudson Orogen.

Sample	Mass (μg)	l[a] (μm)	r[a] (μm)	Ft[b]	U (ppm)	Th (ppm)	eU[c] (ppm)	Sm (ppm)	He (nmol/g)	Raw date (Ma)	Corr date (Ma)
SO-89-49b, augen gneiss; UTM 13V 330000, 6310000											
a1	4.3	193	67	0.78	23.7	2.2	24	95	40.9	299	379
a2	2.8	216	44	0.70	10.5	0.9	11	101	20.6	336	467
a3	3.3	175	47	0.71	19.1	1.7	19	102	33.5	305	422
a4	1.5	123	47	0.69	18.1	0.7	18	175	39.6	378	533
HUD98-31, tonalite; UTM 13U 481478, 6107646											
a2	2.4	174	49	0.72	16.6	3.6	17	168	34.7	348	474
a3	1.8	164	44	0.69	20.6	3.9	21	198	38.4	314	444
a4	2.7	147	55	0.73	11.2	1.1	11	137	17.1	263	353
a5	1.6	144	40	0.66	12.9	1.6	13	194	26.0	339	498
HUD98-40, amphibolite; UTM 13U 503982, 6142270											
a1	1.4	139	34	0.61	16.0	19.4	21	26	31.8	277	448
a2	2.0	107	51	0.71	16.3	25.6	22	67	32.9	264	367
HUD96-31, granite; UTM 13U 458350, 6166050											
a1	4.5	232	52	0.74	4.7	2.6	5	232	10.5	333	437
a2	3.7	238	46	0.71	6.4	5.0	8	288	14.8	332	451
a3	2.0	150	41	0.66	9.7	12.6	13	446	27.8	374	545
a4	2.8	152	53	0.73	5.5	4.1	6	249	10.3	275	369
a5	1.9	153	44	0.68	9.0	10.0	11	379	23.0	346	489
HUD98-49, McLennan meta-arkose; UTM 13V 573094, 6217013											
a1	3.1	154	62	0.76	10.8	1.6	11	118	19.3	302	393
a2	2.6	162	50	0.72	13.9	1.5	14	133	22.8	282	384
a3	1.4	143	38	0.65	13.2	8.1	15	230	20.1	235	355
a7	1.0	101	35	0.60	12.9	9.9	15	458	25.6	290	465

[a] l—length, r—radius.
[b] Ft is alpha-ejection correction of Farley et al (1996).
[c] eU—effective uranium concentration, weights U and Th for their alpha productivity, computed as [U] + 0.235 * [Th].

Table 2
Apatite fission-track data from the western Trans-Hudson Orogen.

Sample	Rock type	Easting northing	Number of grains dated	ρ_s[a] $\times 10^6$ t/cm^2	ρ_i[b] $\times 10^6$ t/cm^2	ρ_d[c] $\times 10^5$ t/cm^2	Central[d] age (Ma) (± 1 S.E.)	P(χ)^2 (%)	Uranium content (ppm)	Mean track[e] length (μm) (± 1 S.E.)	Standard deviation track length
SO-89-49	Augen Gneiss	13V 330000 6310000	20	2.97 (2617)	3.32 (1462)	1.241 (4600)	509.5 ± 24.9	60	32	11.5 ± 0.5 (83)	2.5
HUD96-31	Granite	13U 458350 6166050	20	1.05 (1347)	1.67 (1063)	1.200 (4600)	352.9 ± 19.6	90	17	12.8 ± 0.4 (100)	2
HUD98-31	Tonalite Gneiss	13U 481478 6107646	30	2.22 (3199)	2.06 (1480)	0.953 (4600)	473.6 ± 23.0	99	26	12.2 ± 0.3 (113)	1.8
HUD98-40	Amphibolite	13U 503982 6142270	20	2.8 (1746)	2.49 (778)	0.968 (4600)	498.5 ± 27.4	94	31	12.3 ± 0.4 (100)	1.9
HUD98-49	McLennan Meta-arkose	13V 573094 6217013	20	2.08 (1796)	1.96 (845)	1.008 (4600)	492.0 ± 26.7	55	23	10.8 ± 0.5 (103)	2.4

[a] ρ_s—spontaneous track density. Number in parentheses is the number of tracks counted for ages and fluence calibration or the number of tracks measured for lengths.
[b] ρ_i—induced track density. Number in parentheses is the number of tracks counted for ages and fluence calibration or the number of tracks measured for lengths.
[c] ρ_d—track density in muscovite detector covering CN-6 (1.05 ppm); reported value determined from interpolation of values for detectors covering standards at the top and bottom of the reactor packages. Number in parentheses is the fluence gradient correction.
[d] S.E. = standard error; lf = 1.551×10^{-10} yr^{-1}, g = 0.5; zeta = 4772 ± 300.
[e] Mean track lengths not corrected for length bias (Laslett et al., 1982). Number in parentheses is the number of tracks measured for lengths.

the AFT and AHe dates for the other samples and younger than the corresponding AHe result for this sample. Because this sample is a significant outlier from the other results, we exclude it from further discussion here.

4. Paleozoic–early Mesozoic thermal history patterns across the western Canadian shield

4.1. Approach

We employed the HeFTy modeling program (Ketcham, 2005) to carry out thermal history simulations of the Slave craton, Churchill Province, and THO datasets. We used the radiation damage accumulation and annealing model for apatite He diffusion of Flowers et al. (2009) and the fission-track annealing model of Ketcham et al. (2007). For each simulation, 50,000 random histories satisfying defined time-temperature constraints were generated and predicted dates and track length distributions compared against input dates, eU, grain size, and track length data (Ketcham, 2005). All simulations used random subsegment spacing. We specifically attempted to avoid guiding thermal histories by using broad boxes for our thermal history constraints.

There is ongoing discussion and refinement of different approaches to inverse modeling of thermochronometry data. Separate statistics are used by HeFTy to test the goodness of fit of age and track length distributions (Ketcham, 2005; Ketcham et al., 2009). Others favor a Bayesian approach that assesses the joint likelihood of predicting different parameters (Gallagher, 1995; Gallagher et al., 2009; Stephenson et al., 2006). The choice of approach would not modify the primary conclusion of the thermochronometry simulations described below. Running alternative HeFTy simulations in which we vary the number and nature of the random subsegments yields negligible difference in the results (Figs. 1, S2). For example, allowing or disallowing continuous cooling and changing the number of subsegment parameters from two (Fig. 1B) to five (Fig. 2SC) yields indistinguishable outcomes. Most of our simulations require gradual heating or cooling in Phanerozoic time owing to the relatively slow thermal response expected during deposition and unroofing of sedimentary rocks in this cratonic setting, but we find that permitting the segment parameters to instead be characterized by intermediate heating or cooling rates does not modify our conclusions (compare Figs. 1B and S2C with S2D). Similarly, increasing the minimum surface temperature constraint from 0 °C to 20 °C to account for possibly higher surface temperatures in Paleozoic–Mesozoic time has little impact (compare Figs. 1B and S2B).

4.2. Geologic constraints

The following constraints were used in our thermal history simulations. First, all simulations begin in the Proterozoic to account for the radiation damage accumulated in the apatites during Proterozoic time that would influence the apatite He retentivity in the Phanerozoic. Simulations for the central Churchill Province and western THO study areas begin at ca. 1.7 Ga because several constraints indicate unroofing to near-surface conditions shortly prior to that time (Fig. S2E, F). ^{40}Ar/^{39}Ar mica dates record cooling to <300 °C by 1.78–1.72 Ga in the East Lake Athabasca region of the central Churchill Province (Flowers et al., 2006) and by 1.77 Ga in the western THO (Schneider et al., 2007). The ca. 1.7 Ga Athabasca basin unconformably overlies the basement in northern Saskatchewan, indicating that basement in both study areas was at the surface by that time (Rayner et al., 2005). In the Slave craton the thermal history simulations begin at 1270 Ma (Fig. S2A) because mafic dikes of this age have estimated emplacement depths of 8.5 km, indicating that the rocks were at depths too great for radiation damage accumulation in the apatites at that time (Ault et al., 2009).

Additional thermal history constraints come from two significant, well-documented episodes of burial and unroofing recorded by Paleozoic and Mesozoic sedimentary rocks and unconformities in the Western Canada Sedimentary Basin (Wheeler et al., 1996). First, Lower Devonian units nonconformably overlie the basement to the west of the THO and central Churchill Province study areas. For this reason our models for these areas assume that the basement was at near surface conditions in early Paleozoic time, prior to onset of reburial in the Devonian (Figs. 1C, D, S2E, F). In the Slave craton, additional constraints on this portion of the thermal history are imposed by Cambrian, Ordovician, and Silurian strata preserved in the Western Canada Sedimentary Basin, as well as by Paleozoic sedimentary xenoliths from the southwestern and north-central Slave craton (Figs. 1B, S2A, see Ault et al., 2009 for additional details). Second, Cretaceous units unconformably overlie Precambrian basement and Paleozoic

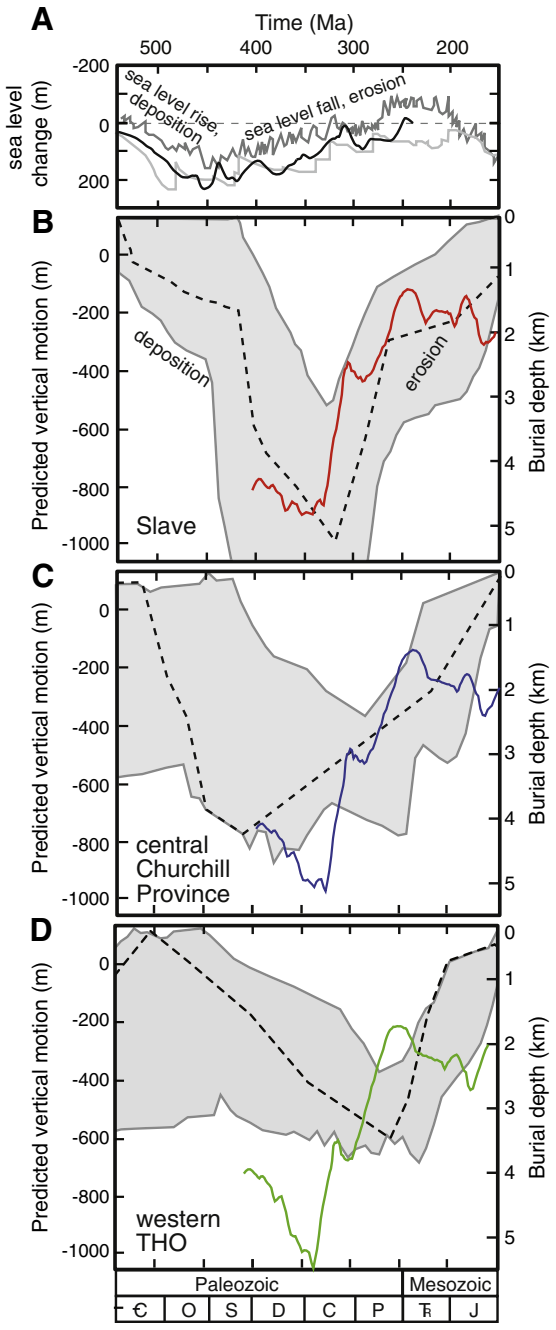

Fig. 2. (A) Paleozoic–early Mesozoic sea level curve reconstructions relative to present day sea level from (Haq and Al-Qahtani, 2005)—black line, (Haq and Schutter, 2008)—dark gray line, (Vail et al., 1977)—light gray line. Positive values are sea levels higher than at present. A negative slope represents sea level rise and inferred deposition of sediments whereas a positive slope depicts sea level fall and associated erosion; the plot is constructed in this way to facilitate comparison with elevation change and burial curves. (B) Slave craton, (C) central Churchill Province, and (D) western THO Paleozoic–early Mesozoic predicted vertical motion histories (refer to left y-axis) compared with the burial and unroofing histories inferred from the thermochronometry data (refer to right y-axis). Predicted vertical motion is the colored line in each plot relative to mean global dynamic topography, which is zero. Negative and positive slopes represent subsidence and surface uplift, respectively. Burial depth histories are shown within the gray shaded domains encompassing thermal histories with good fits to the data, and converted to depths assuming a 0 °C surface temperature and 20 °C/km geotherm. Dashed black lines are best-fit burial curves. Era and period boundaries of the geologic timescale are denoted along the bottom x-axis.

strata in exposures of the Western Canada Sedimentary Basin closest to the three study areas. This observation, as well as additional information gleaned from sedimentary xenolith inclusions in kimberlite pipes of the Slave craton, requires erosion to near-surface conditions by the end of the Jurassic. The simulations impose this constraint, and permit a reburial phase in Cretaceous–Tertiary time prior to unroofing to the surface by the present (Figs. 1, S2). Finally, previous studies in the central portion of the Western Canada Sedimentary Basin concluded that maximum Cretaceous–Early Tertiary burial near the middle of the basin was ~1.1 km and decreased eastward (Nurkowski, 1984; Willett et al., 1997), such that significant Cretaceous aggradation in the central Churchill Province and western THO appears unlikely. For this reason we limit Cretaceous–Tertiary temperatures in those simulations to ≤40 °C (Figs. 1C, D, S2E, F). In contrast, as summarized in Ault et al. (2009), the constraints from the Slave craton do not as strongly imply limited Cretaceous sedimentary accumulation. We therefore permit significant Cretaceous reheating in the Slave craton simulations (Figs. 1B, S2A–D).

4.3. Thermal history simulations and results

The choice of thermochronometry data used in the thermal history simulations of the Slave craton and central Churchill Province datasets are described in detail in Ault et al. (2009) and Flowers (2009), respectively. The simulations of these samples were carried out again here so that all simulations permitted a Cretaceous reburial phase and used a surface temperature of 0 °C. The results are essentially the same as those reported previously (Figs. 1B–C, S2A–E) (Ault et al., 2009; Flowers, 2009). The good fit paths from the Slave craton simulations demand peak Paleozoic temperatures of ≥84 °C. The good fit paths from the central Churchill Province result bracket peak Paleozoic–Mesozoic temperatures between ~62 and 95 °C.

In addition, we carried out simulations of the new AHe and AFT data for the THO samples. We performed joint AHe–AFT simulations for the three samples with AFT data and more than two individual AHe analyses, using two constraints in each simulation: 1) the mean AHe date, 1-sigma sample standard deviation, mean equivalent spherical radius, mean U, and mean Th values of the dated apatites, and 2) the AFT date, asymmetric 2-sigma standard error, and c-axis projected track lengths for the same sample as the second constraint. We used the mean eU values and mean AHe dates for these simulations because there is not significant eU or age variability in the dated apatites from these samples. These simulations yielded both good and acceptable fit paths, with peak Paleozoic temperatures of the good fit paths in all three simulations bracketed between 64 and 80 °C. Figs. 1D and S2F show the simulation results for sample SO89-49 that are representative of those for the other simulated samples from the western THO.

Comparison of thermal history results for the three study areas reveals similar Phanerozoic thermal histories but differences in the peak temperatures attained across the region during a pronounced heating and cooling event in Paleozoic–early Mesozoic time (Figs. 1B to D, S2). The data also permit a second interval of reheating in Cretaceous time, but this is of less relevance for the current study. Regionally, the intensity of Paleozoic reheating was highest in the Slave-Wopmay orogen and likely lower in the central Churchill Province and western THO (peak temperatures of ≥84 °C, 62–95 °C, and 64–80 °C, respectively).

5. Thickness, spatial extent, and evolution of missing portions of the Paleozoic–Mesozoic stratigraphic record in the western Canadian shield

The overall pattern of substantial heating and cooling in Paleozoic–early Mesozoic time is the most robust aspect of our results, and is demanded by the Phanerozoic dates that require temperatures sufficient to induce partial to complete He loss from the apatite crystals, combined with the unconformable relationships and sedimentary xenolith inclusions in kimberlite pipes that indicate erosion to near-

surface conditions first in early Paleozoic time and then by the end of the Jurassic (Cookenboo et al., 1998; Pell, 1996; Wheeler et al., 1996). The conclusion that a widespread heating and cooling event affected the western Canadian shield in Paleozoic–early Mesozoic time has two significant implications.

First, the only reasonable explanation for this pattern is that the craton was substantially buried (heated) by sedimentary rocks in Paleozoic time, followed by significant Paleozoic–early Mesozoic erosion that removed these strata from the rock record across the study region (and induced cooling of the underlying basement rocks). Information on heat flow and geothermal gradients can be used to estimate the magnitude of burial in Paleozoic time required to explain the basement's Paleozoic temperature distribution. Heat flow estimates for the central Slave craton, southwestern Slave craton, and western THO are 46 ± 6 mW/m^2 (Mareschal et al., 1999), ~53 mW/m^2 (Lewis and Wang, 1992), and 37 ± 6 mW/m^2 (Mareschal et al., 2005), respectively. A heat flow map of the Canadian shield in Mareschal and Jaupart (2004) suggests values in the vicinity of our central Churchill Province samples of 42–47 mW/m^2. Anomalously high Wopmay orogen heat flow values of 90 ± 15 mW/m^2 (Lewis et al., 2003) may explain the younger, but still overlapping within uncertainty, AHe dates from Wopmay relative to the Slave craton (Ault et al., 2009).

The modern-day Slave craton, central Churchill Province, and western THO heat flow values are broadly consistent with typical cratonic geothermal gradients of ~20 °C/km (Chapman, 1986). Assuming that the shallow crustal geotherm did not vary dramatically across the Slave, central Churchill, and THO study areas at the time of Paleozoic peak temperature attainment implies that the basement in the northwest was buried more deeply than that to the southeast in Paleozoic time. For example, applying a 20 °C/km geotherm implied by the heat flow data and a 0 °C surface temperature consistent with the modern mean annual temperature in the region indicates Paleozoic burial of basement currently exposed in the Slave craton, central Churchill Province and western THO to depths of ≥4.2 km, 3.1–4.8, and 3.2–4 km, respectively. A lower geotherm or surface temperature assumption increases the inferred Paleozoic depths, and the opposite assumptions reduce the thickness estimates. For example, assuming more extreme geotherms of 15 °C/km or 30 °C/km suggests minimum Paleozoic burial of the Slave craton basement by 5.6 km and 2.8 km, respectively. We recognize that a number of factors can influence the geotherm and cause it to be spatially and temporally variable, including low thermal conductivities of blanketing sediments and variable heat production of the missing section. Although these factors limit the precision of the burial depth estimates, the key point is that any reasonable choice of geotherm demands burial of the cratonic basement in Paleozoic time to explain the thermochronometry data, with the results suggestive of greater burial depths to the northwest. Regardless of the absolute burial magnitude inferred from the data, the question then becomes the nature of the processes responsible for this depositional and erosional history.

The second important implication of the data is that the simplest interpretation of the depositional environment of the missing Paleozoic strata across this 1300 km region is in an offshore or marine setting similar to the preserved Paleozoic remnants in the region. Comparison of our results with other observations reveals a broadly consistent pattern implying that most of the Precambrian basement now exposed in the Canadian shield was flooded and blanketed by marine sedimentary rocks in Paleozoic time. For example, Paleozoic sedimentary xenoliths are entrained within the Cross diatreme of the southwestern Slave craton (Pell, 1996), Devonian marine limestone xenoliths are contained within the Jericho kimberlite pipe of the north-central Slave craton (Cookenboo et al., 1998), and an outlier of Ordovician marine limestone crops out >700 km from continuous correlative exposures in the Western Canada Sedimentary Basin (Wheeler et al., 1996; Wright, 1955) (Fig. 1). AFT datasets in the southern Canadian shield southeast of our study region similarly indicate significant Paleozoic reheating and burial (Feinstein et al., 2009; Kohn et al., 2005). Previous isotopic study of Canadian clastic sedimentary rocks suggested that a <2 km thick succession of shale-dominated rocks was deposited in a marine shelf environment across most of the craton (Patchett et al., 2004) in Devonian time, although our results indicate that the sedimentary package was likely thicker (>3 km) than this estimate.

6. Causative mechanisms for continental-scale burial and unroofing across the western Canadian shield

6.1. Epeirogeny or eustasy?

A limited number of mechanisms can explain a Paleozoic–early Mesozoic history in which the seas inundated and subsequently receded from a vast interior region of the Canadian shield: long-term sea level rise and fall, subsidence followed by uplift of the craton, and interaction of these eustatic and epeirogenic processes. We first examine Paleozoic global sea level curve reconstructions and compare them with the history of burial and erosion inferred from our thermochronometry datasets. Fig. 2A depicts three different sea level chronologies from the beginning of the Paleozoic (545 Ma) to the end of the Jurassic (145 Ma) plotted relative to present day sea level (Haq and Al-Qahtani, 2005; Haq and Schutter, 2008; Miller et al., 2005; Vail et al., 1977). The long term trend of sea level rise and fall is the most reliable aspect of the record (Haq and Schutter, 2008). The chronologies in Fig. 2A share similar long term patterns characterized by rising sea levels during the Cambrian, a peak in the Ordovician with maximum estimates of ~230 m above present day, subsequent declining sea levels until the end of the Triassic, followed by rising sea levels during the Jurassic. The absolute magnitude of sea level change is more difficult to constrain than the long-term trends (Haq and Schutter, 2008) and is likely smaller at least for the Cretaceous sea-level high (Miller et al., 2005; Watts and Steckler, 1979) possibly due to the effects of dynamic topography (Conrad and Husson, 2009; Moucha et al., 2008; Muller et al., 2008; Spasojevic et al., 2008).

The sea level chronologies are compared with our inferred depositional and erosional histories for the western Canadian shield in Fig. 2, where the thermal histories are converted to estimated burial depth histories assuming a 20 °C/km geotherm and 0 °C surface temperature. We focus on the overall trends of the burial-unroofing fields rather than the absolute amplitudes because the first-order patterns are the most robust aspects owing to the geotherm assumptions discussed earlier. This comparison reveals that the long term trend of burial in the ~450 to 350 Ma time interval is coeval with an extended sea level decline. Falling sea levels would induce an erosional rather than a depositional signal in the geological record. The lack of synchroneity between these chronologies therefore suggests that eustasy was not the primary control on the Paleozoic burial and unroofing history in the western Canadian shield.

6.2. Implications for testing mantle dynamic models

The poor correlation between the Paleozoic–Mesozoic history of burial and unroofing with eustatic sea level chronologies suggests that vertical motion of the craton is required to explain the observations. Moreover, the similarity of burial and unroofing patterns at a continental-scale within this plate interior setting, and little to no crustal deformation within the craton at this time, suggests that plate margin tectonism is unlikely to be the cause of elevation change. We therefore explore whether long-wavelength vertical motions induced by dynamic topography provide a viable explanation for the results. Our primary objectives are to evaluate this hypothesis, illustrate the specific approach of comparing directly the temporal patterns of

burial and unroofing with the predicted evolution of dynamic topography in cratonic regions, and assess how this strategy may in turn help constrain mantle dynamic models.

Here we consider a particular dynamic model of thermochemical convection coupled with a proxy model of plate motions since 450 Ma (Lithgow-Bertelloni and Richards, 1998; Scotese, 2001; Zhang et al., 2010) to predict the 400 to 150 Ma change in dynamic topography for the three study areas in the western Canadian shield (Fig. 2B–D colored lines). This model is the first to explore the evolution of Earth's mantle structure associated with supercontinent Pangea assembly and breakup (Zhang et al., 2010). The mantle structures and dynamic topography from reference case FS1 of Zhang et al. (2010) are shown here, with the model setup, techniques, model results, as well as additional cases explained fully in Zhang et al. (this volume). Distinct from most previous studies that considered only the effects of subducted slabs on dynamic topography (e.g., Gurnis, 1993; Mitrovica et al., 1989), our study incorporates both subducted slabs and broad upwellings that evolve dynamically self-consistently following the law of conservation of energy. Although subducted slabs generally exert the first-order control on the dynamic topography of continents, broad and warm mantle upwellings may also have a significant effect, depending on the tectonic setting. For example, the African and Pacific topographic superswells of ~1 km magnitude may be caused by the African and Pacific superplumes (e.g., Cazenave et al., 1989; Davies and Pribac, 1993; Nyblade and Robinson, 1994). Recent studies also indicate that Earth's mantle convection may include as much as 30% basal heating from the core (Lay et al., 2008; Leng and Zhong, 2008), suggesting a significant role of mantle upwellings in mantle dynamics. The role of broad mantle upwellings in producing the present-day African and Pacific superswells and in affecting continental dynamic topography is discussed thoroughly in Zhang et al. (this volume).

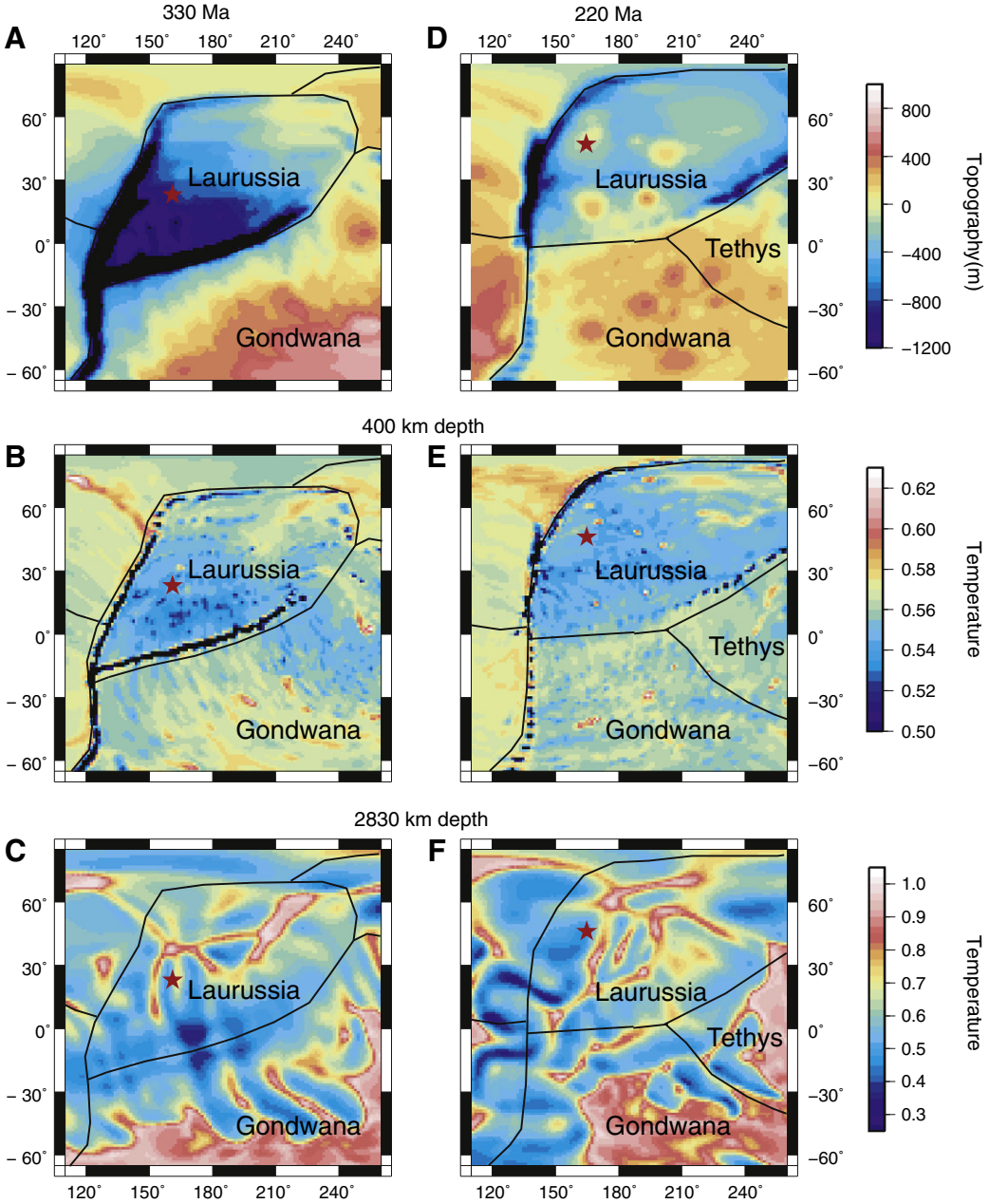

Fig. 3. Dynamic topography (A) and thermal structures at 400 km (B) and 2830 km (C) depths at 330 Ma and those (D, E, and F) at 220 Ma from global model calculations. The red stars represent the location of the Slave craton, the black lines are for plate boundaries.

Fig. 3 shows the modeled dynamic topography and mantle thermal structures at 400 km and 2830 km depths at 330 Ma and 220 Ma (the star shows the location of the Slave craton for reference). At 330 Ma when Gondwana and Laurussia collide to form Pangea, the Slave craton is in a broad region of depressed dynamic topography (Fig. 3A), reflecting the relatively cold mantle due to previous subduction at the south and west sides of Laurussia (Fig. 3B, C). At 220 Ma, the mantle below Laurussia has warmed up significantly (Fig. 3E, F), leading to significant dynamic uplift of the Slave craton (Fig. 3D). Although there are some uncertainties about the nature of the western plate boundary of Laurussia during the Paleozoic and Mesozoic (Ward, 1995), we found that temporal variations of Slave craton dynamic topography remain unchanged for case FS11 in Zhang et al. (2010) in which the age and buoyancy force of subducted slabs on the western side of Laurussia are reduced significantly (Zhang et al., this volume). This result suggests that the vertical motion history of the western Canadian shield during this period of time is largely controlled by subduction at the south side of Laurussia, which is well-constrained. Although the dynamic topography shows short-wavelength variations associated with small mantle upwelling plumes, relatively long-wavelength features are more robust (Zhang et al., this volume). Therefore, we compute spatially averaged dynamic topography over a radius of 1000 km around the three study areas from 400 to 150 Ma and compare it with the inferred burial and unroofing histories in Fig. 2 over that same time interval. Results for averaging dynamic topography over 500 km are similar to those for the 1000 km average.

The predicted vertical motion history of the western Canadian shield is characterized by maximum subsidence in early Paleozoic time followed by long-term surface uplift by 700-800 m through the end of the Paleozoic (Fig. 2B–D). The direction and magnitude of predicted elevation change rather than the absolute values are most important for our comparative analysis. As noted above, this chronology reflects an early Paleozoic low in the dynamic topography of the Canadian shield explained by cold mantle downwellings induced by convergence during Pangea assembly, followed by development of warmer upwellings after the amalgamation of the Pangea supercontinent (Zhang et al., 2010; Zhong et al., 2007) (Fig. 3). These curves differ clearly from the sea level chronologies (Fig. 2). The shift from subsidence to uplift is ~100 Ma later than the sea level zenith in the Ordovician, with the magnitude of predicted vertical motion change (800–900 m) several times greater than the inferred maximum amplitude of sea level change over the same time interval (~250 m). Comparison of the burial depth and predicted vertical motion chronologies, however, reveals that our inferred depositional and erosional histories mimic the elevation change due to dynamic topography predicted by the mantle dynamic models to first order, especially for the Slave craton and central Churchill Province datasets (Fig. 2B–C). Note that burial depth is not a perfect proxy for the amplitude of subsidence because compaction and crustal loading during sediment deposition influence the subsidence history. The most important result of the comparison is that the shift from long term burial to unroofing coincides with the change from subsidence to surface uplift in the predicted vertical motion history. The coincidence of the shift from subsidence and deposition to uplift and erosion is the expected pattern if the modeled timing and magnitude of dynamic topography is correct to first order, because the greater amplitude of dynamic topography change relative to global sea level change suggests that the former should be the dominant control on burial and unroofing. Moreover, the prediction of subsidence followed by 700-800 m of surface uplift should cause sedimentary units deposited during early Paleozoic subsidence to be nearly or entirely eroded away during the later uplift phase, thus matching the history inferred from the thermochronometry data and geological observations across the Canadian shield.

We conclude that dynamic topography is a plausible first order cause of long-wavelength elevation change in this continental interior, and more complete exploration of a broader spectrum of mantle dynamic models will yield additional insights into this problem. Cratonic thermochronometry data can be used to further calibrate this and other mantle models, as well as to isolate other controls on vertical motions and deposition. For example, the commencement of a depositional phase at ~500 Ma in the Canadian shield inferred from geological constraints and our thermochronometry data may help constrain the timing of accumulation of subducted slabs below Laurussia in the dynamic models (e.g., Liu et al., 2008; Muller et al., 2008) that currently only consider the post-450 Ma plate motion history. In addition, an intriguing secondary spatial variability in the depositional and erosional magnitudes is apparent between the three study areas in Fig. 2. Although we infer greater burial and unroofing in the Slave craton than in the study areas to the southeast, the magnitude of elevation change predicted by the dynamic model is comparable in all three locations. Also, the burial and unroofing history for the western THO data does not fit as well with the predicted vertical motion history as in the other two regions. These patterns could be used to explore how the mantle dynamic model parameters or plate tectonic configurations must be refined to fit the secondary spatial variations in the thermochronometry data. Alternatively, the geographic heterogeneity in depositional and erosional patterns may suggest variable tectonic influences across the craton, perhaps due to far-field flexural effects or differences in sediment supply associated with tectonism along the margins of the Canadian shield.

7. Conclusions

Cratonic thermochronometry studies allow for deciphering of cryptic burial and unroofing histories that otherwise have been largely erased from the geologic record in continental interior settings. New and published AHe and AFT data for Precambrian basement from three study areas in the western Canadian shield reveal substantial heating and cooling during Paleozoic–Mesozoic time, indicative of a significant episode of burial and unroofing across an extensive region of the continent that is now mostly devoid of Phanerozoic cover. The results suggest coherent spatial variability in the thickness and history of the missing Paleozoic sequences, and imply a phase of substantial burial before ~350 Ma ($\geq$4.2 km in the Slave craton assuming a typical cratonic geotherm) followed by unroofing between ~350 Ma and 250 Ma. Eustatic sea level change alone is unable to explain our results, instead pointing toward vertical continental displacements as an important control on the depositional and erosional history. We use a three dimensional model of thermochemical convection to explore the evolution of Earth's mantle structure during assembly and breakup of the Pangea supercontinent, and find that the predicted vertical motions due to dynamic topography compare favorably with the burial and unroofing patterns in our dataset. This result supports the notion that mantle flow associated with supercontinent amalgamation and breakup exerts important control on elevation change within “stable” cratonic interior regions. By comparing the history of cratonic burial and unroofing with the dynamic model predictions we are able to push the testing of dynamic models deeper into the past than most previous work (Liu et al., 2008; Muller et al., 2008). Thermochronometry data from the Canadian shield and other continental interior settings can be used to test, calibrate, and further refine this and other mantle dynamic models.

Supplementary data to this article can be found online at doi:10.1016/j.epsl.2011.11.015.

Acknowledgements

This work was supported by NSF grants EAR-0711451 to R.M.F., EAR-1015669 and EAR-1135382 to S.Z., and EAR-9804874 to S.A.K. We thank S. Bowring for generous access to northwestern Canadian shield samples. We appreciate comments from Mike Gurnis and an anonymous reviewer that helped improve the clarity of the manuscript.

References

Algeo, T.J., Seslavinsky, K.B., 1995. The Paleozoic world: continental flooding, hypsometry, and sealevel. Am. J. Sci. 295, 787–822.

Ault, A.K., Flowers, R.M., Bowring, S.A., 2009. Phanerozoic burial and unroofing history of the western Slave craton and Wopmay orogen from apatite (U–Th)/He thermochronometry. Earth Planet. Sci. Lett. 284, 1–11.

Bond, G.C., Kominz, M.A., 1991. Disentangling middle Paleozoic sea level and tectonic events in cratonic margins and cratonic basins of North America. J. Geophys. Res. 96, 6619–6639.

Braun, J., 2010. The many surface expressions of mantle dynamics. Nat. Geosci. 3, 825–833.

Burgess, P.M., Gurnis, M., 1995. Mechanisms for the formation of cratonic stratigraphic sequences. Earth Planet. Sci. Lett. 136, 647–663.

Cazenave, A., Souriau, A., Dominh, K., 1989. Global coupling of Earth surface topography with hotspots, geoid and mantle heterogeneities. Nature 340, 54–57.

Chapman, D.S., 1986. Thermal gradients in the continental crust. In: Dawson, J.B., Carswell, D.A., Hall, J., Wedepohl, K.H. (Eds.), The Nature of the Lower Continental Crust: Geological Society Special Publication, 24, pp. 63–70.

Conrad, C.P., Husson, L., 2009. Influence of dynamic topography on sea level and its rate of change. Lithosphere 1, 110–120.

Cookenboo, H.O., Orchard, M.J., Daoud, D.K., 1998. Remnants of Paleozoic cover on the Archean Canadian Shield: limestone xenoliths from kimberlite in the central Slave craton. Geology 26, 391–394.

Davies, G.F., Pribac, F., 1993. Mesozoic seafloor subsidence and the Darwin Rise, past and present. In: Pringle, S., et al. (Ed.), The Mesozoic Pacific. Geology, Tectonics, and Volcanism, Geophysics Mono, 77. AGU, Washington, D.C, pp. 39–52.

Farley, K.A., Wolf, R.A., Silver, L.T., 1996. The effect of long alpha-stopping distances on (U–Th)/He ages. Geochim. Cosmochim. Acta k60, 4223–4229.

Feinstein, S., Kohn, B.P., Osadetz, K., Everitt, R., O'Sullivan, P., 2009. Variable Phanerozoic thermal history in the southern Canadian shield: evidence from an apatite fission-track profile at the Underground Research Laboratory (URL), Manitoba. Tectonophysics 475, 190–199.

Flowers, R.M., 2009. Exploiting radiation damage control on apatite (U–Th)/He dates in cratonic regions. Earth Planet. Sci. Lett. 277, 148–155.

Flowers, R.M., Mahan, K.H., Bowring, S.A., Williams, M.L., Pringle, M.S., Hodges, K.V., 2006. Multistage exhumation and juxtaposition of lower continental crust in the western Canadian Shield: linking high-resolution U–Pb and 40Ar/39Ar thermochronometry with P-T-D paths. Tectonics 25.

Flowers, R.M., Ketcham, R.A., Shuster, D.L., Farley, K.A., 2009. Apatite (U–Th)/He thermochronometry using a radiation damage accumulation and annealing model. Geochim. Cosmochim. Acta 73, 2347–2365.

Gallagher, 1995. Evolving temperature histories from apatite fission-track data. Earth Planet. Sci. Lett. 136, 421–435.

Gallagher, K., Charvin, K., Nielsen, S., Sambridge, M., Stephenson, J., 2009. Markov chain Monte Carlo (MCMC) sampling methods to determine optimal models, model resolution and model choice for Earth Science problems. Mar. Pet. Geol. 26, 525–535.

Godey, S., Deschamps, F., Trampert, J., Snieder, R., 2004. Thermal and compositional anomalies beneath the North American continent. J. Geophys. Res. 109, B01308.

Gurnis, M., 1993. Phanerozoic marine inundation of continents driven by dynamic topography above subducting slabs. Nature 364.

Hager, B.H., Richards, M.A., 1989. Long-wavelength variations in Earth's geoid: physical models and dynamical implications. Philos. Trans. R. Soc. Lond. 328, 309–327.

Haq, B.U., Al-Qahtani, A.M., 2005. Phanerozoic cycles of sea-level change on the Arabian Platform. GeoArabia 10, 127–160.

Haq, B.U., Schutter, S.R., 2008. A chronology of Paleozoic sea-level changes. Science 322, 64–68.

Hoffman, P.F., 1989. Precambrian geology and tectonic history of North America. In: Bally, A.W., Palmer, A.R. (Eds.), The Geology of North America — An overview. Geological Society of America, Boulder, CO, pp. 447–512.

Kelley, S.A., Chapin, C.E., Corrigan, J., 1992. Mesozoic to Cenozoic cooling histories of the flanks of the northern and central Rio Grande rift, Colorado and New Mexico. N. Mex. Bur. Mines Miner. Resour. Bull. 145, 39.

Ketcham, R.A., 2005. Forward and inverse modeling of low temperature thermochronometry data. In: Reiners, P.W., Ehlers, T.A. (Eds.), Reviews in Mineralogy and Geochemistry: Low-temperature thermochronology: Techniques, interpretations, and applications. Mineralogical Society of, America, pp. 275–314.

Ketcham, R.A., Carter, A.C., Donelick, R.A., Barbarand, J., Hurford, A.J., 2007. Improved modeling of fission-track annealing in apatite. Am. Mineral. 92, 799–810.

Ketcham, R.A., Donelick, R.A., Balestrieri, M.L., Zattin, M., 2009. Reproducibility of apatite fission-track length data and thermal history reconstruction. Earth Planet. Sci. Lett. 284, 504–515.

Kohn, B.P., Gleadow, A.J.W., Brown, R.W., Gallagher, K., Lorencak, M., Noble, W.P., 2005. Visualizing thermotectonic and denudation histories using apatite fission-track thermochronology. In: Reiners, P.W., Ehlers, T.A. (Eds.), Reviews in Mineralogy and Geochemistry: Low-temperature thermochronology: Techniques, interpretations, and applications. Mineralogical Society of, America, pp. 527–565.

Laslett, G.M., Kendall, W.S., Gleadow, A.J.W., Duddy, I.R., 1982. Bias in measurement of fission-track length distributions. Nucl. Tracks Radiat. Meas. 170, 79–85.

Lay, T., Hernlund, J., Buffett, B.A., 2008. Core–mantle boundary heat flux. Nat. Geosci. 1, 25–32.

Leng, W., Zhong, S.J., 2008. Controls on plume heat flux and plume excess temperature. J. Geophys. Res. 113, B04408. doi:10.1029/2007JB005155.

Lewis, T.J., Wang, K., 1992. Influence of terrain on bedrock temperature. Glob. Planet. Chang. 98, 87–100.

Lewis, T.J., Hyndman, R.D., Flock, P., 2003. Heat flow, heat generation, and crustal temperatures in the northern Canadian Cordillera: thermal control of tectonics. J. Geophys. Res. 198, 2316–2334.

Lithgow-Bertelloni, C., Gurnis, M., 1997. Cenozoic subsidence and uplift of continents from time-varying dynamic topography. Geology 25, 735–738.

Lithgow-Bertelloni, C., Richards, M.A., 1998. Dynamics of Cenozoic and Mesozoic plate motions. Rev. Geophys. 36, 27–78.

Liu, L., Spasojevic, S., Gurnis, M., 2008. Reconstructing Farallon Plate subduction beneath North America back to the Late Cretaceous. Science 322, 934–938.

Mareschal, J.C., Jaupart, C., 2004. Variations of surface heat flow and lithospheric thermal structure beneath the North American craton. Earth Planet. Sci. Lett. 223, 65–77.

Mareschal, J.C., Jaupart, C., Cheng, L.Z., Rolandone, F., Gariepy, C., Bienfait, G., Guillou-Frottier, L., Lapointe, R., 1999. Heat flow in the Trans-Hudson Orogen of the Canadian Shield: Implications for Proterozoic continental growth. J. Geophys. Res. 104, 29,007–29,024.

Mareschal, J.C., Jaupart, C., Rolandone, F., Gariepy, C., Fowler, C.M.R., Bienfait, G., Carbonne, C., Lapointe, R., 2005. Heat flow, thermal regime, and elastic thickness of the lithosphere in the Trans-Hudson Orogen. Can. J. Earth Sci. 42, 517–532.

Miller, K.G., Kominz, M.A., Browning, J.D., Wright, J.D., Mountain, G.S., Katz, M.E., Sugarman, P.J., Cramer, B.S., Christie-Blick, N., Pekar, S.F., 2005. The Phanerozoic record of global sea-level change. Science 310, 1293–1298.

Mitrovica, J.X., Beaumont, C., Jarvis, G.T., 1989. Tilting of continental interiors by the dynamical effects of subduction. Tectonics 8, 1079–1094.

Moucha, R., Forte, A.M., Mitrovica, J.X., Rowley, D.B., Quere, S., Simmons, N.A., Grand, S.P., 2008. Dynamic topography and long-term sea-level variations: there is no such thing as a stable continental platform. Earth Planet. Sci. Lett. 271, 101–108.

Muller, R.D., Sdrolias, M., Gaina, C., Steinberger, B., Heine, C., 2008. Long-term sea-level fluctuations driven by ocean basin dynamics. Science 319, 1357–1362.

Nurkowski, J.F., 1984. Coal quality, rank variation, and its relation to reconstructed overburden, Upper Cretaceous and Tertiary plains coals, Alberta, Canada. AAPG Bull. 68, 285–295.

Nyblade, A.A., Robinson, S.W., 1994. The African superswell. Geophys. Res. Lett. 21, 765–768. doi:10.1029/94GL00631.

Patchett, P.J., Embry, A.F., Ross, G.M., Beauchamp, B., Harrison, J.C., Mayr, U., Isachsen, C.E., Rosenberg, E.J., Spence, G.O., 2004. Sedimentary cover of the Canadian shield through Mesozoic time reflected by Nd isotopic and geochemical results for the Sverdrup Basin, arctic Canada. J. Geol. 112, 39–57.

Pell, J.A., 1996. Kimberlites in the Slave structural province, NWT, Canada. The Gangue: Geological Association of Canada: Mineral Deposits Division, 51, pp. 1–3.

Pysklywec, R.N., Mitrovica, J.X., 2000. Mantle flow mechanisms of epeirogeny and their possible role in the evolution of the Western Canada Sedimentary Basin. Can. J. Earth Sci. 37, 1535–1548.

Rayner, N.M., Stern, R.A., Bickford, M.E., 2005. Tectonic implications of new SHRIMP and TIMS U–Pb geochronology of rocks from the Sask Craton, Peter Lake Domain, and Hearne margin, Trans-Hudson Orogen, Saskatchewan. Can. J. Earth Sci. 42, 635–657.

Ricard, Y., Fleitout, L., Froidevaux, C., 1984. Geoid heights and lithospheric stresses for a dynamical Earth. Annu. Geophys. 2, 267–286.

Ricard, Y., Richards, M., Lithgow-Bertelloni, C., Stunff, Y.L., 1993. A geodynamic model of mantle density heterogeneity. J. Geophys. Res. 98, 21895–21909.

Schneider, D.A., Heizler, M.T., Bickford, M.E., Wortman, G.L., Condie, K.C., Perilli, S., 2007. Timing constraints of orogeny to cratonization: Thermochronology of the Paleoproterozoic Trans-Hudson orogen, Manitoba and Saskatchewan, Canada. Precambrian Res. 153, 65–95.

Scotese, C.R., 2001. Atlas of Earth History. PALEOMAP Progress Report 90–0497. Dept. of Geol., Univ. of Tex, at Arlington, Texas.

Sleep, N.H., 1976. Platform subsidence mechanisms and “eustatic” sea-level changes. Tectonophysics 36, 45–56.

Sloss, L.L., 1963. Sequences in the cratonic interior of North America. Geol. Soc. Am. Bull. 74, 93–114.

Spasojevic, S., Liu, L., Gurnis, M., Muller, R.D., 2008. The case for dynamic subsidence of the U.S. east coast since the Eocene. Geophys. Res. Lett. 35, L08305. doi:10.1029/02008GL033511.

Spasojevic, S., Liu, L., Gurnis, M., 2009. Adjoint models of mantle convection with seismic, plate motion, and stratigraphic constraints: North America since the Late Cretaceous. Geochem. Geophys. Geosyst. 10, Q05W02. doi:10.1029/2008GC002345.

Stephenson, J., Gallagher, K., Holmes, C., 2006. A Bayesian approach to calibrating apatite fission track annealing models for laboratory and geological timescales. Geochim. Cosmochim. Acta 70, 5183–5200.

Vail, P.R., Mitchum Jr., R.M., Thompson III, S., 1977. Seismic stratigraphy and global changes in sea level. Part 4: global cycles of relative changes of sea level. Mem. Am. Assoc. Pet. Geol. 26, 83–97.

Ward, P.L., 1995. Subduction cycles under western North America during the Mesozoic and Cenozoic eras. Geol. Soc. Am. Spec. Pap. 299, 12.

Watts, A.B., Steckler, M.S., 1979. Subsidence and eustasy at the continental margin of eastern North America. In: Series, M.E. (Ed.), Deep Drilling Results in the Atlantic Ocean: Continental Margins and Paleoenvironment. American Geophysical Union, pp. 218–234.

Wheeler, J.O., Hoffman, P.F., Card, K.D., Davidson, A., Sanford, B.V., Okulitch, A.V., Roest, W.R., 1996. Geological Map of Canada. Geological Survey of Canada, “A” Series Map 1860A.

Willett, S.D., Issler, D.R., Beaumont, C., Donelick, R.A., Grist, A.M., 1997. Inverse modeling of annealing of fission tracks in apatite 2: application to the thermal history of the Peace River Arch Region, Williston Basin. Am. J. Sci. 297, 970–1011.

Wright, G.M., 1955. Geological notes on central District of Keewatin, Northwest Territories. Geol. Surv. Can. Pap. 55–17, 8–12.
Wright, G.N., McMechan, M.E., Potter, D.E.G., 1994. Structure and architecture of the Western Canada Sedimentary Basin. In: Mossop, G.D., Shetson, I. (Eds.), (Comp.), Geological Atlas of the Western Canada Sedimentary Basin Canadian Society of Petroleum Geologists and Alberta Research Council, Calgary, Alberta.
Zhang, N., Zhong, S., Leng, W., Li, Z.-X., 2010. A model for the evolution of the Earth's mantle structure since the Early Paleozoic. J. Geophys. Res. 115, 1–22.
Zhang, N., Zhong, S., Flowers, R.M., this volume. Predicting and testing continental vertical motion histories since the Paleozoic. Earth and Planetary Science Letters.
Zhong, S., Zhang, N., Li, Z.-X., Roberts, J.H., 2007. Supercontinent cycles, true polar wander, and very long-wavelength mantle convection. Earth Planet. Sci. Lett. 261, 551–564.